Widespread reliance of rainfed crops on upwind irrigated agriculture in India

Authors

Akash Koppa[1,2,*]
Francesca Bassani[1]
Jessica Keune[3]
Victoria Deman[4]
Damian Insua-Costa[4]
Vittal Hari[5]
Subimal Ghosh[6]
Diego G. Miralles[4]
Sara Bonetti[1,*]

Affiliations

[1] Laboratory of Catchment Hydrology and Geomorphology, School of Architecture, Civil and Environmental Engineering, EPFL Valais Wallis, Sion, Switzerland
[2] Department of Environmental Science & Technology, University of Maryland, College Park, United States
[3] European Centre for Medium-Range Weather Forecasts, Bonn, Germany
[4] Hydro-Climate Extremes Lab (H-CEL), Ghent University, Ghent, Belgium
[5] Department of Environmental Science and Engineering, Indian Institute of Technology (ISM) Dhanbad, Dhanbad, India
[6] Department of Civil Engineering, Indian Institute of Technology Bombay, Mumbai, India
[*] Authors to whom any correspondence should be addressed.

Corresponding Authors

Akash Koppa; Sara Bonetti
Email: akoppa@umd.edu, sara.bonetti@epfl.ch

Preprint Status Statement

This manuscript is a **non-peer-reviewed preprint** submitted to **EarthArXiv**. The manuscript is **currently under consideration for peer review at *Environmental Research Letters***.

Crossmark

RECEIVED
dd Month yyyy

REVISED
dd Month yyyy

LETTER

Widespread reliance of rainfed crops on upwind irrigated agriculture in India

Akash Koppa[1,2,*], Francesca Bassani[1], Jessica Keune[3,*], Victoria Deman[4,*], Damian Insua-Costa[4,*], Vittal Hari[5,*], Subimal Ghosh[6,*], Diego G. Miralles[4,*], Sara Bonetti[1,*],

[1]Laboratory of Catchment Hydrology and Geomorphology, School of Architecture, Civil and Environmental Engineering, EPFL Valais Wallis, Sion, Switzerland
[2]Department of Environmental Science & Technology, University of Maryland, College Park, United States
[3]European Centre for Medium-Range Weather Forecasts, Bonn, Germany
[4]Hydro-Climate Extremes Lab (H-CEL), Ghent University, Ghent, Belgium
[5]Department of Environmental Science and Engineering, Indian Institute of Technology (ISM) Dhanbad, Dhanbad, India
[6]Department of Civil Engineering, Indian Institute of Technology Bombay, Mumbai, India
*Authors to whom any correspondence should be addressed.

E-mail: akoppa@umd.edu, sara.bonetti@epfl.ch

Keywords: Land–atmosphere interactions, irrigated and rainfed agriculture, atmospheric moisture recycling

Abstract

Rainfed crops account for approximately 40% of India's food production and support 60% of its livestock. Although linked to oceanic monsoon rainfall, their productivity also depends on terrestrial evaporation, particularly in the non-monsoon season. However, the degree to which rainfed crops also rely on moisture sourced from upwind irrigated areas, remains largely unknown. Using a combination of models and observations, we show that upwind irrigated crops contribute 7%±6% of the rainfall over rainfed areas, rising to 15%±10% during the pre-monsoon months. In the absence of this input, water stress experienced by rainfed crops can increase by 5–10% during the crucial mid to late crop growth phases, potentially affecting yields. Our results reveal an unrecognized atmospheric link between irrigated and rainfed agriculture, which is overlooked in current agricultural policies. Planning and managing these systems in an holistic manner can help strengthen regional food and water security under future climates.

1 Introduction

More than a billion hectares of land are cultivated with rainfed crops globally [1, 2], supporting the livelihood of ∼2.5 billion people [3]. They account for ∼60% of the world's food production and more than 90% of the total farmed land in the socio-economically vulnerable parts of sub-Saharan Africa, Latin America, and Asia [4]. In India, with over 140 million hectares of sown area (60% of the total area under cultivation), rainfed agriculture plays a crucial role in ensuring the country's food security [5]. By definition, the productivity of rainfed crops depends on the intensity and timing of precipitation. In India, this implies that rainfed crops are disproportionally tied to the variability of monsoon rainfall (July–September), which contributes 70% of the country's annual rainfall [6, 7]. Furthermore, a significant proportion of rainfed crops in India are also grown in post-monsoon months (October–December), during which crop growth is supported primarily by residual soil moisture from the monsoonal rainfall. During the monsoon season, it has been observed that even a 10–15% deficit in rainfall reduces food grain production by up to 10 million tonnes [8]. For example, crop losses during the severe drought of 2002 caused the country's gross domestic product (GDP) to decline by 1% (equivalent to ∼$5 billion) [9].

The prevailing understanding is that rainfall in India is largely sourced from oceanic evaporation, transported inland from the Arabian Sea and the Bay of Bengal by large-scale coupled ocean-atmosphere oscillations at decadal to subseasonal timescales [10, 11, 12, 13, 14, 15, 16, 17, 18]. Although this dependency suggests a strong link between ocean evaporation and rainfed crop productivity in India, atmospheric moisture over the subcontinent is not solely derived from oceanic sources. Recent evidence suggests that terrestrial evaporation also plays an important role in sustaining rainfall over India through moisture recycling [19]. Such

sources of moisture are also crucial for sustaining the growth of rainfed crops during the non-monsoon season.

Among the various land-based sources, including trees, short vegetation, soil, and lakes, irrigation is a significant contributor to land–atmosphere fluxes [20]. From the Great Plains in the United States [21] to the Gezira Scheme in East Africa [22] and even the large-scale irrigation expansion in India [23, 24, 25], several modelling and observation-based studies have shown that irrigation significantly impacts both local and remote rainfall patterns, from subdaily [26] to climatological [27] time scales. Irrigation as a source of moisture, especially over rainfed regions, is particularly relevant in India due to the close geographical proximity between irrigated and rainfed crops. This proximity increases the likelihood of recycled moisture from upwind irrigation precipitating over rainfed crops. This is exemplified by the Indo-Gangetic Plain (IGP), one of the most intensively irrigated regions in the world [28], where large-scale irrigation occurs adjacent to areas with extensive rainfed cropping, and exhibits a high degree of moisture recycling [29, 30]. The potential for irrigation-driven evaporation to contribute to rainfall over rainfed crops is particularly valuable during the non-monsoon season, when oceanic moisture transport is weaker and rainfall is more limited compared to the monsoon season. With a significant proportion of the rainfed crops grown in the non-monsoon season, irrigation contribution to rainfall might be crucial for supporting the growth of rainfed crops. Despite its potential significance, the extent to which rainfed crops rely on moisture sourced from evaporation in upwind irrigated regions remains poorly quantified to date.

To evaluate the potential reliance of rainfed crops on upwind irrigation agriculture in India, we formulate the following hypothesis (Fig. 1): Evaporation from irrigated crops in upwind regions reduces water stress in rainfed crops by enhancing rainfall via atmospheric moisture recycling. Here, water stress is represented in terms of evaporative stress, which is defined as the degree to which crop water demand is satisfied by soil moisture (see Methods). To test this hypothesis, we use an observation-constrained moisture tracking framework capable of identifying the spatiotemporal source of rainfall (see Methods). Specifically, we track the trajectories of simulated air parcels that result in rainfall over rainfed regions (sink region in Fig. 1) backward in time over 15 days to quantify the contribution of upwind evaporation (source region in Fig. 1), over the years 2000–2020. This upwind contribution is evaluated both in terms of (a) blue water evaporation (E_{blue}), defined as the part of the total water used by crops that can be directly attributed to applied irrigation, and (b) both blue and green water (E_{green}), which is the part of total crop evaporation which can be attributed to rainfall. With a Food and Agriculture Organisation (FAO 56)-based model [31, 32], we explicitly estimate blue and green evaporation from 14 major irrigated and rainfed crops in India (see Methods for details and the complete list of crops considered in the study). Finally, we assess the importance of upwind irrigation to rainfed crops by recalculating evaporative stress under a counterfactual scenario where the irrigation contribution to rainfall over rainfed regions is removed.

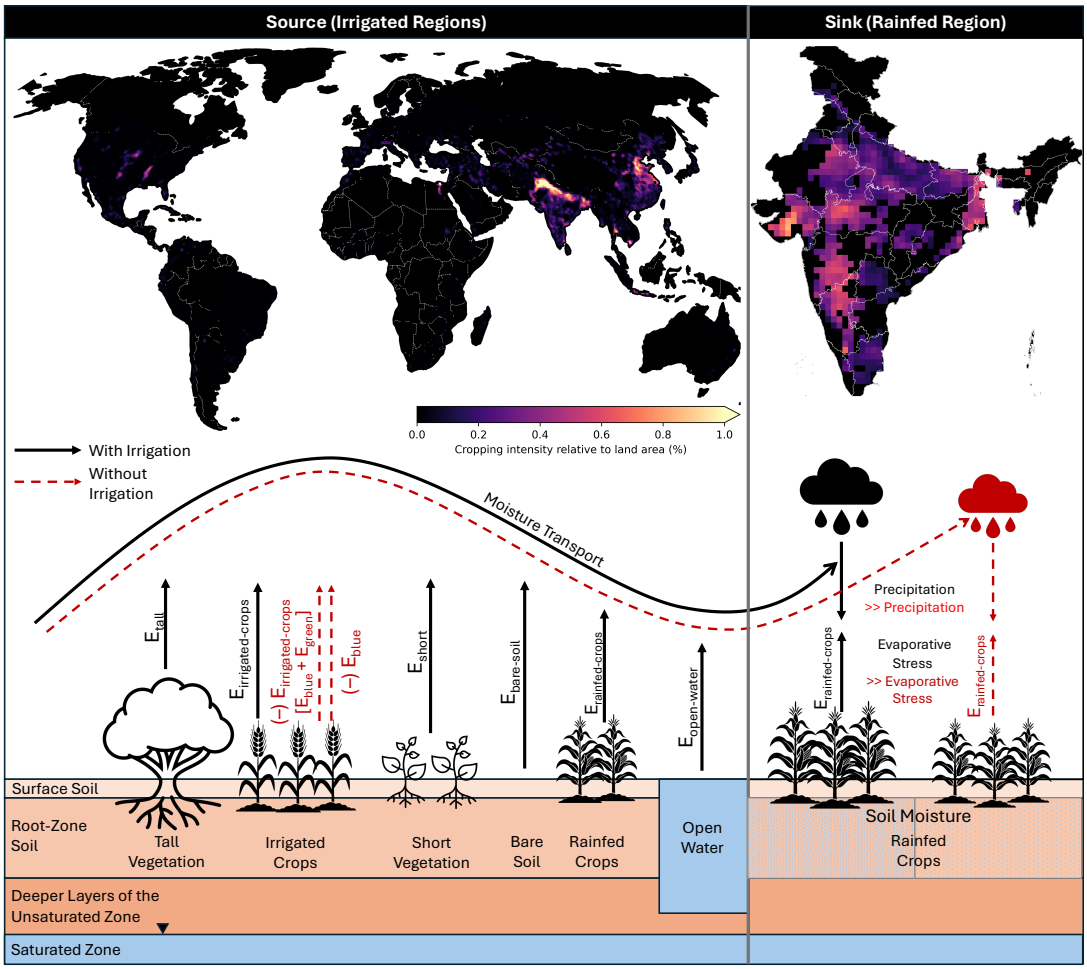

Figure 1. Conceptual representation of the atmospheric link between upwind irrigated agriculture and rainfed crops.
A schematic of an idealized scenario in which irrigated agriculture is practiced upwind (referred to as 'source regions') of an area with rainfed crops (referred to as 'sink region'). In addition to irrigated crops, the upwind regions might include rainfed crops, natural vegetation (tall and short), bare soil, and open water (lakes and oceans). The water evaporated from the upwind irrigated regions increases the moisture content or relative humidity of the local atmosphere. This enhanced moisture is advected downwind and provides additional moisture for rainfall over rainfed regions, contributing indirectly to soil water available for rainfed crops. Thus, rainfed crops can be considered to rely on upwind irrigated agriculture if their absence (red dashed line) leads to a considerable decrease in crop evaporation (higher evaporative stress) due to the lower rainfall and consequent decline in soil moisture in rainfed regions. Evaporation from irrigated crops consists of two components, both of which are considered in this study: (a) blue water (E_{blue}) sourced from the applied irrigation water and (b) green water (E_{green}) sourced from rainfall over irrigated crops.

2 Methods

2.1 Identifying and quantifying the sources of rainfall over rainfed regions

To identify and quantify the land and oceanic sources of rainfall over rainfed regions and to determine the contribution of irrigated crops (both E_{green} and E_{blue}) and irrigation water (only E_{blue}), the following steps are taken. First, a Lagrangian atmospheric model forced with an atmospheric reanalysis dataset is used to simulate the trajectories of air parcels distributed across the globe. In the next step, the air parcel trajectories that result in rainfall over the target region (rainfed areas in this case) are tracked backward in both time and space. Along the trajectory of the air parcel, the moisture gained (through evaporation) and lost (through precipitation) are considered. Finally, these moisture uptakes and losses are bias-corrected with observation-based estimates and aggregated to determine the contribution of upwind evaporation to rainfall over rainfed regions. In the next section, we first describe the Lagrangian atmospheric model used in the study and then detail the moisture tracking framework used to evaluate the air parcels and attribute moisture contributions from irrigated crops to rainfall over rainfed regions.

2.1.1 Atmospheric transport model simulations For the global simulations of air parcel trajectories, the model used in this study is the Flexible Particle Dispersion model (FLEXPART) version 10.4 [33, 34] forced with the ERA5 atmospheric reanalysis data [35]. The model simulations are carried out at a global scale using approximately 10 million air parcels which are uniformly distributed throughout the globe and are tracked forward both in space and time. The following variables are used to force FLEXPART v10.4: temperature, specific humidity, horizontal and vertical wind, cloud cover, precipitation, 2-m air temperature, dew-point temperature, sensible and latent heat fluxes, and North/South and West/East surface stress. The model tracks the location (latitude, longitude, and height) of each of the 10 million parcels and simulates their dynamic and thermodynamic properties (e.g., temperature, density, specific humidity). Using ERA5 reanalysis data as forcing, these outputs are available at 3-hourly timesteps.

2.1.2 Moisture tracking framework FLEXPART simulations described above are used to construct and evaluate the trajectories of air parcels, that is all air parcels residing over each of the grid cells representing the rainfed regions (Fig. 2a) are tracked backward in time for 15 days and parsed for precipitation in the rainfed regions to identify moisture sources in previous time steps and locations. In doing so, all the locations in which the air parcel gains or loses moisture are tracked. In this study, the analysis of air parcel trajectories from the FLEXPART simulations are carried out using a recently developed moisture tracking framework [36]. Within the framework, the trajectories are evaluated using the following three steps (described below): (a) diagnosis, (b) attribution, and (c) bias-correction. For a detailed description of the three steps, please refer to Appendix A.

2.2 Observation, reanalysis, and satellite-based datasets
Various reanalysis and satellite-based datasets are used for constraining the modelling framework described above. The FLEXPART v10.4 model is forced with ERA5 reanalysis [35] at 0.5° spatial resolution. Variables at single and multiple model levels (137-levels) extending from the surface to the top of the atmosphere are used. The data spans the entire globe, and is available at 0.25° spatial resolution. Here, three-hourly reanalysis products and the lowest 90 model levels are used for forcing the FLEXPART v10.4 model over a time period of 21 years (2000–2020). For the bias-correction of precipitation, we use the Multi-Source Weighted Ensemble Precipitation, version 2 (MSWEP v2.8) dataset [37]. The MSWEP dataset is available at a spatial resolution of 0.1° and a 3-hourly timestep. To bias-correct evaporation from land surface, the Global Land Evaporation Amsterdam Model (GLEAM) version 4.0a is used [38]. This dataset is available at 0.1° at daily temporal resolution, spanning the years of 1980–Present. For ocean evaporation, we use the Objectively Analysed Air-Sea Fluxes (OAFlux) dataset [39]. The spatial and temporal resolution of OAFlux is 1° and daily respectively. All the datasets are bilinearly interpolated to 0.5°, the resolution at which the final analysis is carried out.

2.3 Modelling crop evaporation
To estimate evaporation from irrigated and rainfed crops, a modelling framework [40, 32] based on the FAO-56 [31] model is employed. Using the model, evaporation from the following 14 major crops in India are estimated: Barley, Cotton, Groundnut, Maize, Millet, Potato, Pulses, Rapeseed, Rice, Sorghum, Soy, Sugarcane, Sunflower, and Wheat. For details of the model, please refer to Appendix B. Using the model, the evaporative stress in crops satisfied by moisture contribution from upwind irrigated agriculture is calulated using the methdology described in Appendix C. Additionally, we also define an irrigation recycling efficiency metric to quantify the value of irrigation applied in a particular region for remote or downwind rainfed crops (refer to Appendix D for details).

3 Results and Discussions

3.1 Upwind irrigated crops as a source of rainfall for rainfed crops
In India, irrigated and rainfed crops are grown in close geographical proximity to each other. To accurately reflect this, in our analysis we consider all 0.5°x0.5° grid cells in which rainfed and irrigated crops each occupy more than 10% of the total land area (Fig. 2a). We make sure that the contribution from upwind irrigated crops to rainfall is estimated for months in which rainfed crops are grown in downwind regions (see Methods). Averaged over the period 2000–2020 and across all the rainfed crop growing regions in India, evaporation from upwind irrigated crops (both E_{blue} and E_{green}) contributes 7.0%±5.2% (53.8±45 mm/year) of the rainfall over rainfed areas. However, we observe large spatial variability in the contribution of upwind irrigated crops to rainfall across the

country. In the Indo-Gangetic Plain (IGP), a northern region with significantly high irrigation intensity compared to the rest of the country, the contribution of upwind irrigated crops is greater than 20%. The interannual variability of the contributions is also high, with an average standard deviation across India of 9.3%±4.5% (Fig. S2), and exhibiting a spatial gradient similar to that of mean values (Fig. 2a).

Next, we isolate the part of the rainfall over rainfed crops that can be attributed only to E_{blue} (i.e., applied irrigation water) in upwind irrigated crop. In Fig. 2b, we see that the E_{blue} contribution to rainfall is between 30–50% of the total contribution (E_{blue}+E_{green}), with a maximum contribution of approximately 6%. Spatially, we observe that in addition to the IGP, E_{blue} contributions are significant in the dry western parts of India (Fig. S3). The relationship between irrigated water (E_{blue}) and irrigated crop (both E_{blue} and E_{green}) evaporation does not show any discernible pattern with monthly rainfall amount or the cropping intensity of rainfed crops (Fig. 2b).

When the evaporation contributions to rainfall from upwind irrigated crops are aggregated monthly, we observe the emergence of a distinct seasonal pattern (Fig. 2c). First, the contribution of evaporation from upwind irrigated crops (both E_{blue} and E_{green}) is the least during the monsoon season (June–September), which is associated not only with the largest proportion of annual rainfall, but also with the highest cropping intensity of rainfed crops (inverted barplots in Fig. 2c). This is expected as rainfall is the primary source of water even for irrigated crops during the monsoon season, which is reflected in the low contribution of E_{blue} (blue-colored stacked barplot) compared to E_{green} (green-colored stacked barplot) in that period. Despite low contributions from upwind E_{blue}, evaporation from irrigated crops contribute as high as 20% to rainfall over rainfed crops in some regions of India (Fig. S4) during the non-monsoon season. This highlights the importance of recycled moisture from land for enhancing rainfall even during the wettest months [41, 19, 42].

While the monsoonal rainfall in India supports the biggest cropping season (termed as "Kharif"), rainfed crops are also grown in the non-monsoon months of October–March (termed as "Rabi") and March–June (termed as "Zaid"). From our analysis it emerges that, during the non-monsoon season, the reliance of rainfall over rainfed regions on upwind irrigated crops are considerably higher than in the monsoon season (Fig. 2c). Spatially, the enhanced relative contribution during the non-monsoon season is consistent across the country with the highest increase seen in the IGP region (Fig. S3). However, during the months of October–December, contribution from upwind E_{green} is considerably higher than E_{blue}, similarly to the monsoon season despite the significantly lower rainfall. The discrepancy between E_{green} and E_{blue} contributions is in line with the fact that, in India, rainfed crops post-monsoon rely on soil moisture gained during the monsoon season [43, 44], in addition to the winter rainfall. Applied irrigation (E_{blue}) plays an important role in sustaining rainfall over rainfed crops during the pre-monsoon months of February–May, where rainfall amounts are the lowest (Fig. 2c). During these months, mean E_{blue} contribution reaches a maximum of 8% in March. Notwithstanding the fact that rainfed cropping intensity in these months is relatively low (maximum 20%), irrigated crops in the upwind areas still represent a very important source of moisture for sustaining downwind rainfall and ensuring rainfed crop production.

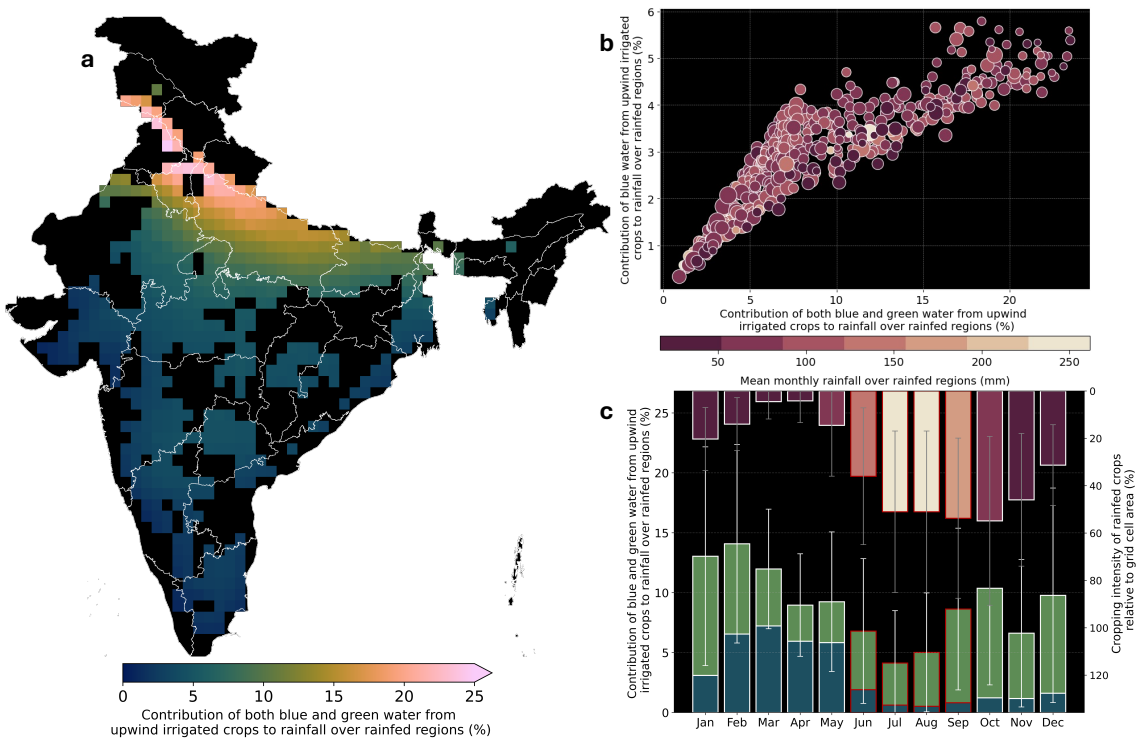

Figure 2. Contribution of evaporation from upwind irrigated crops to rainfall over rainfed crops.
a, Map of India showing the annual mean percentage of rainfall over rainfed crops which is sourced from water evaporated from irrigated crops (both blue and green water) grown in upwind regions, estimated over the years 2000–2020. Note: Selected grid cells, depicted in the figure, represent areas in India demonstrating close proximity of irrigated and rainfed crops: each selected cell is characterized by a minimum of 10% rainfed and 10% irrigated crop land area. **b**, Scatter plot with the contribution of both blue and green water to rainfall over rainfed regions on the x-axis and just the blue water contribution on the y-axis for each grid cell in Fig.2a. The size of the markers correspond to the cropping intensity of rainfed crops in each grid cell and the color represents the mean monthly rainfall over the region. **c**, Stacked barplots showing the seasonality of the contribution of blue (in blue color) and green water (in green color) from upwind irrigated crops to rainfall over rainfed crops. The error bars represent one standard-deviation in upwind irrigated crop contribution. The secondary axes show the seasonality of the cropping intensity of rainfed crops. The color of the bars in the secondary axis represents the mean rainfall over each month. The red boundary highlights the monsoon season (June–September) in India.

3.2 Dependence of rainfed crop evaporative stress on upwind irrigated crops

The previous section established irrigated crop evaporation as an important source of moisture for rainfall over rainfed crops. Here, we explore the extent to which rainfed crops depend on this moisture source to satisfy their water demand. Such an analysis is necessary as the translation of rainfall to rainfed crop evaporation is not linear, i.e., a unit decrease in rainfall does not necessarily imply an unit decrease in crop evaporation given that crop water availability is mediated by soil conditions. To conduct this analysis, we develop two counterfactual scenarios in which (a) both the E_{blue} and E_{green} contribution and (b) only E_{blue} contribution from upwind irrigated crops are removed from rainfall over rainfed crops. Then, the reduced rainfall is used to simulate the evaporation from rainfed crops (see Methods for more details). Each counterfactual scenario is compared with the control one (see Methods) to determine the increase in evaporative stress in the absence of upwind irrigated agriculture (Fig. 3).

Averaged across the 21 years (2000–2020), the evaporative stress increase due to the absence of E_{blue} and E_{green} contribution from upwind irrigated crops is 1.5%±1.0%. Spatially, the highest increase is seen in the IGP (as high as 8%) (Fig. 3a), consistent with the distribution of rainfall contribution estimates already observed in Fig. 2a. Accounting for interannual variability, the average evaporative stress in the IGP region can be as high as 15% (standard deviation of evaporative stress increase is presented in Fig. S6). The average impact of just the blue water component on rainfed crop evaporative stress is insignificant, with values even in the IGP region reaching maximum 1.5% (Fig. 3b). Furthermore, the evaporative stress increases are highest

during the non-monsoon season (Fig. 3c), consistent with the irrigated crop contribution to rainfall in Fig. 3c. In the post-monsoon season (October–December), the availability of moisture from upwind E_{green} is more important than E_{blue} contributions to rainfall in satisfying the water demand of rainfed crops. The situation reverses during the pre-monsoon (February–May), where the applied irrigation (E_{blue}) forms a key source of moisture for downwind rainfed crops.

However, temporally and seasonally averaged estimates of evaporative stress are not entirely indicative of how important upwind crop evaporation is for rainfed crops and their water use. This is because water stress (represented here by evaporative stress) impacts various phases of crop growth differently. To explore this further, we estimate the 90th percentile increase in daily evaporative stress in the absence of contributions from upwind E_{blue} and E_{green} (Fig. S7a). In the absence of irrigated crops, the 90th percentile evaporative stress is 4.7%±3.4% on average across the whole country. This implies that for 36 days in a year, rainfed crops experience three times more water stress than the annual mean. In the IGP region, the 90th percentile evaporative stress is greater than 15% (also about three times the annual mean), with just the E_{blue} contribution reaching the 10% (Fig. S7b). While the 90th percentile results show that plants exhibit high water stress for a significant period of time in the absence of upwind irrigated crops, it does not provide information on 'when' the crops experience it. To better understand the timing of high water stress in the absence of upwind irrigated agriculture, we aggregate the evaporative stress increase estimates of all the grid cells into the four main crop growth phases [31]: (a) initial, (b) crop development, (c) mid-season, (d) late season. From Fig. 4, it is evident that the highest evaporative stress is experienced by the crops during the mid and late seasons of crop growth. Incidentally, these seasons are widely recognized as being the most crucial for crop productivity. While water stress during the mid season can lead to reduced biomass due to reduced photosynthesis [45, 46], in the late season, it can result in reduced grain size and thus a major reduction in crop yields [47, 48]. We note that the increase in evaporative stress due to upwind irrigated crop evaporation presented here represents the upper limit of water stress that can be expected in the complete absence of any evaporation (blue or green) upstream. However, in reality, this might not be the case as the absence of irrigated crops still implies that there might be evaporation from other land covers such as bare soil, grass, or trees (in place of irrigated crops).

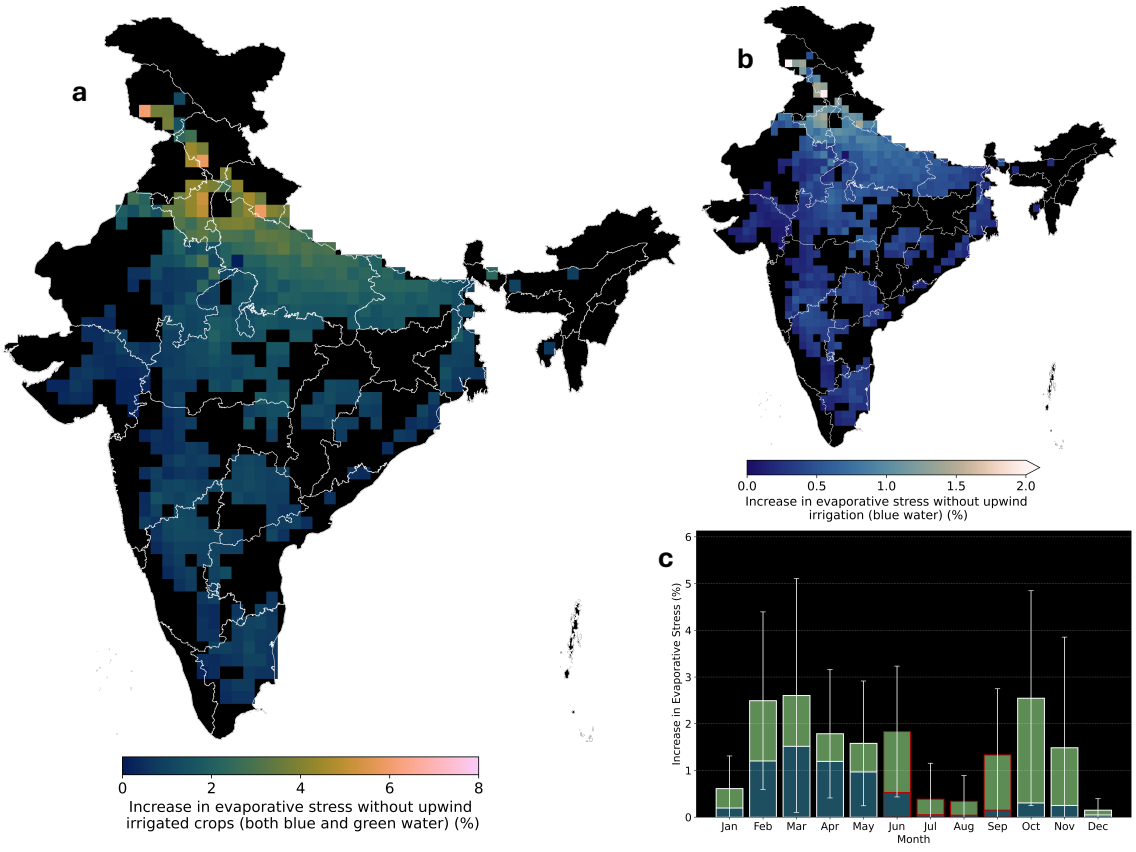

Figure 3. Increase in evaporative stress in rainfed crops in the absence of upwind irrigated crops.
a, Map of India showing the mean percentage increase in evaporative stress in rainfed crops if there were no irrigated crops in the upwind regions thus resulting in a decline in rainfall over rainfed regions (averaged over the years 2000–2020). In estimating these values, both the green and blue water components of evaporation from irrigated crops to precipitation were set to zero. **b**, The mean percentage increase in evaporative stress in rainfed crops due to the absence of contribution from just irrigation (blue water) in the upwind regions to rainfall over them. **c**, Stacked barplots showing the seasonality of the increase in evaporative stress in rainfed crops due to the absence of blue (in blue color) and green (in green color) water contributions to rainfall over them. The error bars represent one standard-deviation in evaporative stress increase across the rainfed crop regions.

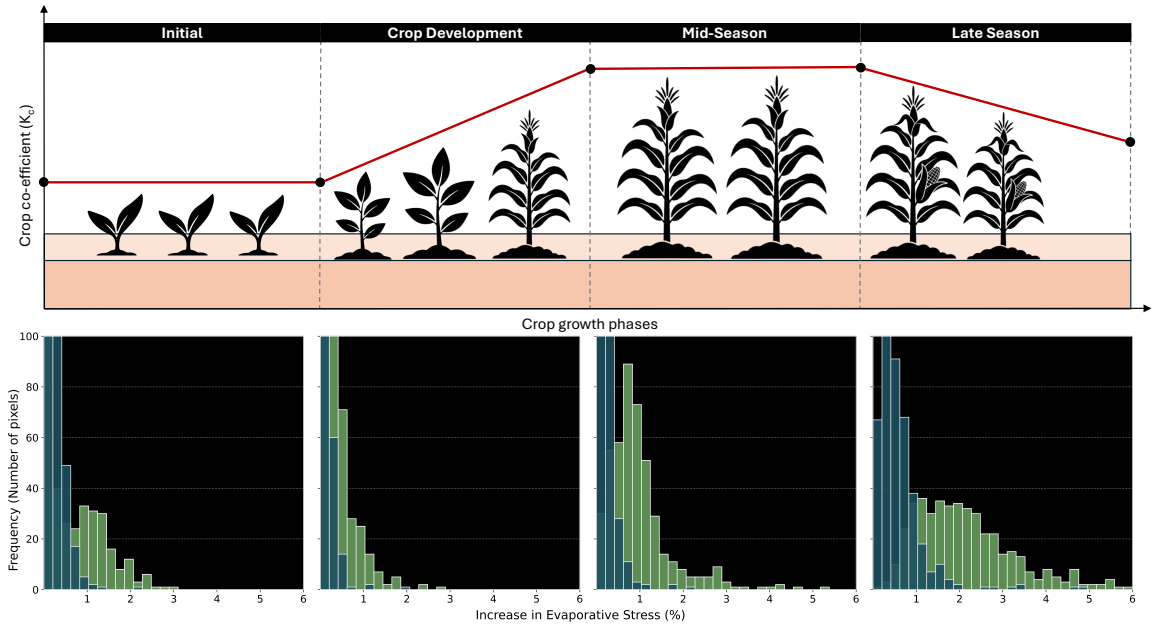

Figure 4. Increase in evaporative stress during different crop growth phases. A schematic (top panel) shows the four different crop growth phases, namely initial, crop development, mid-season, late season. The crop coefficient K_c is the fraction of reference evaporation that is actually evaporated by the crop, and determines the water use of crops at different stages of growth. Bottom panels show the histograms of percentage increase in evaporative stress in rainfed crops corresponding to each crop growth phase, when there are no irrigated crops in the upwind region (both green and blue water, shown in green color) and in the absence of only irrigation (blue water, shown in blue color).

3.3 Irrigation recycling efficiency

Our results, so far, highlighted the potential for irrigated agriculture to supplement the water requirement of downwind rainfed crops. However, given that India is a vast country, a critical question pertinent to policy and planning arises: where should irrigation be expanded or new projects be concentrated such that rainfed crops can derive the maximum benefit from atmospheric recycling? To answer this question we define an irrigation recycling efficiency metric (see Methods), which shows the fraction of applied irrigation that is recycled into a region with substantial rainfed crop presence (at least 10% of the land area is covered by rainfed crops) (Fig. 5a). Our analysis reveals that, in addition to parts of the IGP, western and southwestern parts of India emerge as prominent hotspots for efficient irrigation recycling. Crucially, many of these hotspot areas are not currently as heavily irrigated as the IGP. In other words, an expansion of irrigation in these areas holds the highest potential to support downwind rainfed agriculture by enhancing rainfall over them. Seasonally, we see that the irrigation recycling efficiency varied between 5%–15%. While this may seem modest, its value is higher than the average during the pre-monsoon months (up to 12.5%), during which any additional rainfall is vital for crop growth (Fig. 5b).

Beyond supporting remote rainfed crops, atmospheric moisture recycling also creates a potential benefit for irrigated crops themselves. Evaporated irrigation water can precipitate back over the same or nearby irrigated regions, inducing a positive feedback loop that reduces the net demand for irrigation from surface or groundwater sources. To quantify this self-sustaining effect, we estimate the additional irrigation water that would be needed in the absence of this local recycling. Our results show that this feedback conserves up to 0.05 km^3 of water annually in the intensively irrigated IGP region alone (Fig. 16c). This volume represents a potential direct saving in both water resources and the energy required for pumping.

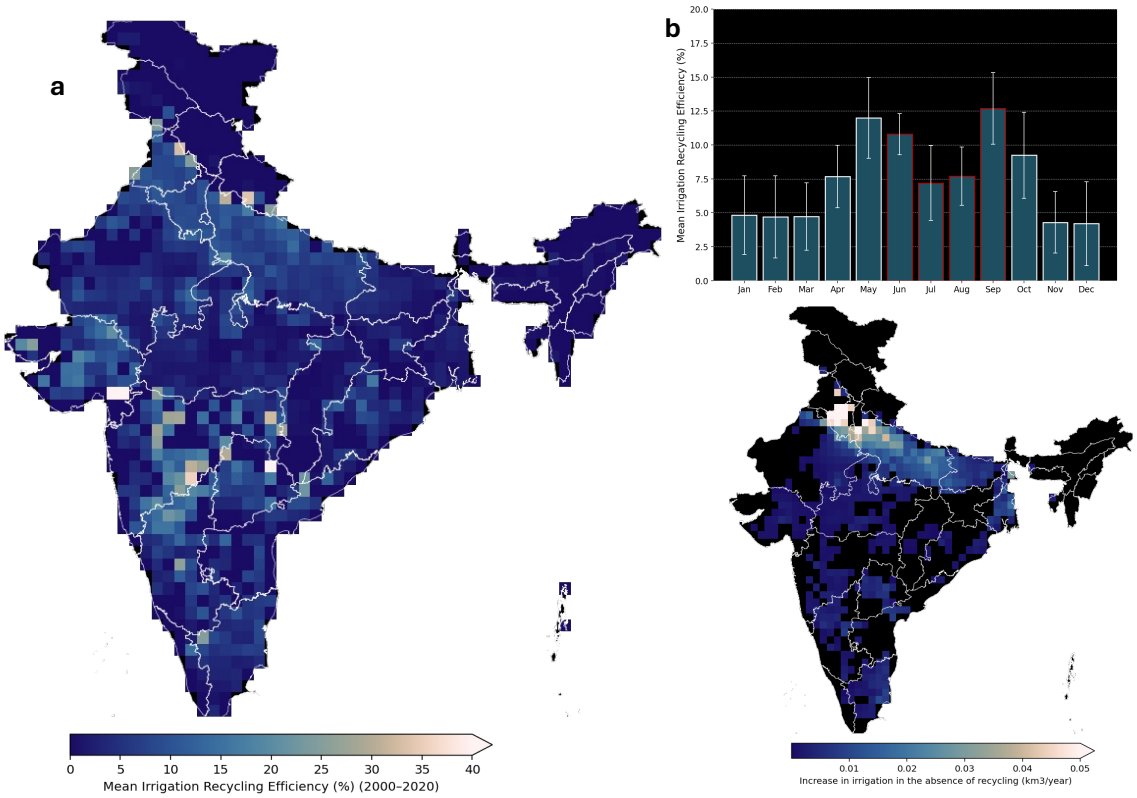

Figure 5. Irrigation recycling efficiency.
a Map of India showing the mean irrigation recycling efficiency (see Methods for a definition) for all the irrigated regions, estimated over the years 2000–2020. **b** Barplots showing the seasonality of irrigation recycling efficiency across all the irrigated regions in India. The red boundary represents the monsoon months in India (June–September). **c** Map of India showing the additional irrigation water needed to compensate for the reduced rainfall over irrigated areas in the absence of atmospheric recycling of applied irrigation water.

4 Conclusions

Irrigated and rainfed agriculture are typically treated as distinct systems in most major agriculture and water management policies. In fact, large-scale capital investments and policy interventions are primarily targeted towards irrigated agriculture, thus creating imbalanced incentive structures that promote irrigation at the cost of supporting rainfed agriculture. In India, these policies include power subsidies for irrigated agriculture [49] and monetary incentives to transition rainfed regions into irrigated areas [50]. In recent decades, there have been increasing calls for planning irrigated and rainfed crop systems in an integrated manner [51]. While existing studies and policies focus on bridging the socio-economic link between them, here we show that irrigated and rainfed agriculture are physically connected through atmospheric moisture recycling. This tight link is especially important in countries, where irrigated and rainfed crops are grown in close proximity to each other, such as India. Specifically, we show that this atmospheric link is particularly relevant in the non-monsoon season, and especially crucial for reducing water stress during the mid and late seasons of crop growth, which are critical phases to determine final crop yields.

We note that the value of upwind irrigated crops for rainfed crop growth quantified in this study is a conservative estimate, given that the analysis was carried out using irrigated crop maps from the year 2000 [28]. However, Asia, and especially northwest India, has witnessed a significant expansion of irrigated area in the last two decades [52] (∼14% by area), pointing to a higher reliance of rainfed crops on upwind irrigation than estimated here. Furthermore, irrigation amounts are estimated based on the deviation of soil moisture from field capacity, a widely used methodology in large scale studies[53, 54]. Thus, we do not take into account region specific irrigation practices which might be important in accurately representing moisture recycling during the monsoon season [55]. Finally, by estimating the degree to which irrigation applied in a certain region recycles into a rainfed crop area (irrigation recycling efficiency), our study provides an actionable pathway through which irrigated and rainfed agriculture can be planned and managed

together. Studies have shown that irrigation expansion can sustainably expand into 35% of the global land area currently under rainfed crops [52, 56]. Thus, the value of atmospheric moisture recycling of evaporation from irrigated crops as an important source of water for sustaining downwind rainfed crops is expected to only increase in the future.

Acknowledgments
The computational resources used in this work was provided by the high performance computing clusters at EPFL in Switzerland (SCITAS), the University of Maryland College Park in the United States (Zaratan), and the Flemish Supercomputing Center in Belgium (VSC). S.B. and F.B. acknowledge support from the Swiss National Science Foundation (grant 10000638) and the Enterprise for Society Center. D.G.M. and V.D. acknowledges the support of the European Research Council (ERC) via the HEAT Consolidator grant (101088405).

Data availability
The data required for reproducing the results and figures of the study are available at https://doi.org/10.5281/zenodo.17238978[57]. FLEXPART-ERA5 simulations of air parcel trajectories are available upon request from the Hydro-Climate Extremes Lab (H-CEL), Ghent University (please contact Victoria Deman, victoria.deman@ugent.be). All other datasets are publicly available (refer to specific studies cited in the text). The code used for producing the figures and the heat and moisture tracking tool used for evaluating the air parcel trajectories are available at

https://doi.org/10.5281/zenodo.17238978[57].

Appendix A. Moisture tracking framework
This section describes the three main components of the moisture tracking framework used to identify and quantify the sources of moisture in the study: (a) diagnosis (b) attribution, and (c) diagnosis.

In the diagnosis step, a dataset of process (rainfall and evaporation) detection is generated by evaluating *all* global two-step trajectories. Thus, for every air parcel and every time step in the global FLEXPART simulations, precipitation (P) and evaporation (E) are detected from changes in specific humidity based on the following mass balance:

$$e - p = m * \Delta q \tag{1}$$

where e and p (both in kg) represent net gains and losses in specific humidity for each parcel from evaporation and precipitation, respectively. m is the mass of the parcel (kg). Δq is the change in specific humidity ($kg.kg^{-1}$) of the parcel between two consecutive time steps along a parcel's trajectory. A parcel is assumed to contribute to a rainfall event if it undergoes a net loss of specific humidity between consecutive time steps ($\Delta q < 0$) and the mean relative humidity (RH) is higher than 80% [58], following the convection parameterization [59]. Then, rainfall over a specific area (A) can be estimated by integrating over individual contributions of all the air parcels n as

$$P = \frac{1}{A}\sum_{i}^{n} \Delta q_i(\Delta q_i < 0kg.kg^{-1}, RH_i > 80\%) \tag{2}$$

Similarly, E is identified if the air parcel experiences a net gain of specific humidity between two consecutive time steps ($\Delta q > 0$) and the parcel resides within the atmospheric boundary layer (ABL). Integrating contributions from every air parcel, E over an area (A) is estimated as:

$$E = \frac{1}{A}\sum_{i}^{n} \Delta q_i(\Delta q_i > 0kg.kg^{-1}, z_i < h_{ABL}^{max}) \tag{3}$$

where, z_i is the height of the parcel (m) and h_{ABL}^{max} is the maximum height of the ABL between the two time steps considered. Finally, the accuracy and reliability of the P and E detection is evaluated using multiple criteria [36].

In the attribution step, the detection criteria ($RH_i > 80\%$ and h_{ABL}^{max}) detailed above are used to identify the air parcels that contribute to rainfall over the rainfed crops regions. Every parcel within the rainfed region which satisfies the P detection criteria is tracked back in time for a maximum of 15 days, which includes the long tail of the distribution of the residence time of atmospheric water vapor [60]. All moisture gains and losses experienced by the parcel along its trajectory are identified. Then, a quantitative attribution of evaporation in the upwind moisture

source regions to rainfall over rainfed regions is carried out. This is a non-trivial task as the moisture uptake experienced by the air parcel can be lost as rain *en route* to the rainfed region, and rain events have to be discounted using an objective criteria. Here, we adopt the method of linear discounting [58] which assumes that the air is well-mixed at all times. Therefore, it is assumed that the moisture lost at a particular time step ($t = i$) in the parcel trajectory has originated from moisture taken up in previous time steps ($t < i$), and the contribution of moisture uptake to the rainfall at time step $t = i$ is proportional to the magnitude of moisture uptakes in the previous time steps. Using this method, the fractional contribution of each source region to the sink region rainfall is calculated by discounting all *en route* losses. This procedure allows us to establish a mass-conserving source–sink relationship that describes the contribution of surface evaporation in the source region to precipitation in the sink region.

Finally, biases arising from uncertainties in P and E detection criteria are corrected using the accuracy information estimated in the diagnosis step with observations of evaporation and precipitation in the source and sink regions, respectively. Additionally, as ERA5 data does not accurately represent evaporation from irrigated and rainfed crops, we chose another observation-based data set to accurately account for crop evaporation (see below). First, evaporation from the moisture source region is bias-corrected using the unconditional E flux calculated using all the air parcels over the source region (from the diagnosis step) and satellite-based E. At this stage, the decomposition of the evaporation estimates in the source region (see below) is used to partition the contribution of upwind evaporation among its various components including: (a) transpiration from natural vegetation (tall and short), (b) bare soil, (c) rainfed crops, and (d) irrigated crops. Furthermore, estimating the green and blue water components of irrigated crop evaporation, we can then attribute the specific contributions of upwind irrigated crops to rainfall over rainfed crops. Then, the rainfall over rainfed regions is bias-corrected using observational estimates (see below) and the contributions from the different source regions are proportionally scaled. The bias-corrections are carried out on a daily timescale. A detailed description of the different datasets used for rainfall, evaporation from oceans, and different natural land cover (tall and short vegetation, bare soil), and crops are presented in the next two sections.

Append B. Crop evaporation model

Evaporation from each of the 14 crops considered in the study, over a single growing season (LGP), is estimated by summing up the daily actual evaporation over the growing season,

$$E_{cr,LGP} = \sum_{j=1}^{LGP} E_{cr,j}, \tag{4}$$

where the daily crop evaporation is calculated as [31]

$$E_{cr,j} = k_{c,cr,j} \cdot k_{s,cr,j} \cdot E_{0,j}, \tag{5}$$

$E_{0,j}$ being the daily potential evaporation, j the day of the growing period, while k_c and k_s are the crop and water stress coefficients, respectively. The daily potential evaporation is derived from GLEAM4 daily potential evaporation, corresponding to short vegetation. The crop coefficient k_c varies during the growing season as

$$k_{c,j} = \{ k_{c,ini} \quad if j \in StageI \tag{6}$$

$$j \cdot \frac{k_{c,mid} - k_{c,ini}}{j - l_I} \quad if j \in StageII \tag{7}$$

$$k_{c,mid} \quad if j \in StageIII \tag{8}$$

$$j \cdot \frac{k_{c,end} - k_{c,mid}}{j - l_I - l_{II} - l_{III}} \quad if j \in StageIV$$

(9)

where the length of each stage (l_{st}) is computed as a fraction (p_{st}) of the length of the growing period. Values of the crop coefficients and length of the crop development stages were obtained from the literature [31] (refer to [32] for more details).

The water stress coefficient k_s varies between 0 (maximum water stress) and 1 (no water stress) and is evaluated considering rainfed and irrigated production separately. For the irrigated production the water stress coefficient is set to 1 (no stress) for the entire duration of the growing period, while for rainfed production it is evaluated as

$$k_{s,j} = \frac{TAW_j - D_{mo,j}}{TAW_j - RAW_j} \tag{10}$$

where TAW [mm] is the total available water content in the root zone, RAW [mm] the readily available water content, and D_{mo} [mm] is the root zone depletion in the morning (i.e., water shortage relative to field capacity). TAW depends on the available water contents AWC [mm/m] and the root depth $Z_{r,j}$ [m] as

$$TAW_j = AWC \cdot Z_{r,j}. \tag{11}$$

The available water content was taken from the Harmonized World Soil database v1.2, while maximum root depth ($Z_{r,max}$) for each crop were obtained from ref. [31]. The root depth was assumed to linearly increase during the first two growing stages and then maintained constant until harvesting.

RAW is the water that crops use for evaporation before water stress and stomata closure begins and is given by

$$RAW_j = \rho \cdot TAW_j \tag{12}$$

where ρ is the depletion fraction coefficient (here assumed constant over the growing season). Values of ρ for each crop were obtained from ref. [31]. In rainfed crops, the root zone depletion in the morning $D_{mo,j}$ is equal to the depletion recorded at the end of the previous day $D_{ev,j-1}$ minus the daily precipitation value P_j,

$$D_{mo,j} = D_{ev,j-1} - P_j. \tag{13}$$

Daily precipitation was obtained by uniformly distributing the monthly rainfall along the growing season with daily frequency. In the evening the root zone depletion decreases because of evaporation as $D_{ev,j} = D_{mo,j} + ET_{cr,j}$, with $E_{cr,j} = k_c \cdot \frac{TAW_j - D_{mo,j}}{TAW_j - RAW_j} \cdot E_{0,j}$. Note that losses by deep percolation are neglected and capillary rise is assumed equal to zero. Furthermore, water excess leading to negative $D_{mo,j}$ is cut off at zero (exceeding precipitation is assumed to be lost as surface runoff). In rainfed conditions, the water volume transpired by the crop during the growth period is totally green ($E_{g,LGP} = E_{LGP}$). Conversely, in irrigated conditions, the daily volume of irrigation, I_j, is determined assuming that the crop fully transpires with no water stress as $I_j = D_{mo,j} - RAW_j + k_{c,j}E_{0,j}$. In the evening, the root zone depletion is given by $D_{ev,j} = D_{mo,j} + E_{cr,j} - I_j$. Thus, the blue water corresponds to the irrigation water ($E_{b,j} = I_j$) while the green water is the difference between the total E and $E_{b,j}$.

We note that, in the analysis here, no specific assumptions about irrigation methods were made – the right amount (not more, not less) of water needed to ensure no stress condition is computed and considered as local irrigation requirement. For rice cultivation, we considered an additional volume per unit area of 200 mm, following the approach by ref.[40]. This allows us to account for the water used to prepare the paddy fields by saturating the root zone in the month before sowing or transplanting.

Appendix C. Evaporation stress estimation

To estimate the degree to which evaporation from upwind irrigated crops reduce the evaporative or water stress in rainfed crops, we compare the evaporation estimates from the control simulation where in irrigated crops are grown in the upwind regions and irrigation is applied (termed here as $E_{r,control}$, where r stands for rainfed crops), with evaporation from two counterfactual scenarios: (a) Complete absence of upwind irrigated crop evaporation (both E_{green} and E_{blue} are present) (b) Absence of just irrigation in the upwind regions (only E_{green} is present). For the first scenario, the contribution from both upwind E_{green} and E_{blue} are removed from rainfall over each of the rainfed grid cell, and the evaporation from rainfed crops are recalculated for all the 14 rainfed crops using

the modeling framework described above (termed here as $E_{r,noIC}$, where IC stands for irrigated crops). The same procedure is repeated for the second scenario with only the upwind E_{blue} contribution removed from rainfall over rainfed crops (termed here as $E_{r,noIW}$, where IW stands for irrigation water). Then, increase in evaporative stress is given by

$$\Delta E = \frac{(E_{control} - E_{r,x}) * 100}{E_{control}} \tag{14}$$

where x can be $noIC$ or $noIW$ depending on which of two scenarios is being considered.

A similar approach is used to determine the increase in irrigation that would be required if there was no atmospheric moisture recycling over irrigated regions. Here, the volume of irrigation applied when irrigated crops are exposed to actual rainfall is the control scenario (termed here as $V_{control}$, where i stands for irrigated crops). Furthermore, only one counterfactual scenario is considered, that is absence of local and upwind irrigation or E_{blue} contribution to rainfall over irrigated crop. After removing the upwind and local E_{blue} contribution to rainfall, the applied volume of irrigation is recalculated (termed here as V_{noIW}). Then, the increase in irrigation volumes is estimated as

$$\Delta V = \frac{(V_{control} - V_{noIW}) * 100}{V_{control}} \tag{15}$$

Appendix D. Irrigation recycling efficiency

Irrigation recycling efficiency (termed here as η) is defined as the fraction of the applied irrigation water which recycles through atmospheric pathways to contribute to rainfall over a region with rainfed crops. For example, if 100 units of water is applied as irrigation in a certain region and if 50 units of water contributes to rainfall over rainfed regions, η is 50%). η is given by

$$\eta = \frac{(V_{i2r}) * 100}{V_{upwind}} \tag{16}$$

where, V_{i2r} is the volume of E_{blue} from upwind irrigated crops that contributes to rainfall over rainfed crops, V_{upwind} is the sum of volumes of irrigation water applied to irrigated crops in the upwind of the rainfed region of interest.

References

[1] Biradar, C. M. *et al.* A global map of rainfed cropland areas (gmrca) at the end of last millennium using remote sensing. *International Journal of Applied Earth Observation and Geoinformation* **11**, 114–129 (2009). URL https://www.sciencedirect.com/science/article/pii/S0303243408000834.

[2] Monfreda, C., Ramankutty, N. & Foley, J. A. Farming the planet: 2. geographic distribution of crop areas, yields, physiological types, and net primary production in the year 2000. *Global Biogeochemical Cycles* **22** (2008). URL https://agupubs.onlinelibrary.wiley.com/doi/abs/10.1029/2007GB002947.

[3] Food Agriculture Organisation of the United Nations (FAO). The state of food and agriculture 2014. https://www.fao.org/family-farming/detail/en/c/273649/ (2014). [Accessed 25-07-2025].

[4] Wani, S. P., Sreedevi, T., Rockström, J. & Ramakrishna, Y. Rainfed agriculture-past trends and future prospects. In *Rainfed agriculture: Unlocking the potential*, 1–35 (CABI Wallingford UK, 2009).

[5] Srinivasa Rao, C. *et al.* Chapter four - potential and challenges of rainfed farming in india. vol. 133 of *Advances in Agronomy*, 113–181 (Academic Press, 2015). URL https://www.sciencedirect.com/science/article/pii/S0065211315001091.

[6] Bhatla, R., Ghosh, S., Verma, S., Mall, R. K. & Gharde, G. R. Variability of monsoon over homogeneous regions of india using regional climate model and impact on crop production. *Agric. Res.* **8**, 331–346 (2019).

[7] Parthasarathy, B., Munot, A. A. & Kothawale, D. R. All-India monthly and seasonal rainfall series: 1871?1993. *Theor. Appl. Climatol.* **49**, 217–224 (1994).

[8] Gadgil, S. & Gadgil, S. The indian monsoon, gdp and agriculture. *Economic and political weekly* 4887–4895 (2006).

[9] Niranjan Kumar, K., Rajeevan, M., Pai, D., Srivastava, A. & Preethi, B. On the observed variability of monsoon droughts over india. *Weather and Climate Extremes* **1**, 42–50 (2013). URL https://www.sciencedirect.com/science/article/pii/S2212094713000078.

[10] Chowdary, J. S., Xie, S.-P. & Nanjundiah, R. S. Chapter 1 - drivers of the indian summer monsoon climate variability. In Chowdary, J., Parekh, A. & Gnanaseelan, C. (eds.) *Indian Summer Monsoon Variability*, 1–28 (Elsevier, 2021). URL https://www.sciencedirect.com/science/article/pii/B978012822402100020X.

[11] Krishnamurthy, L. & Krishnamurthy, V. Decadal scale oscillations and trend in the indian monsoon rainfall. *Clim. Dyn.* **43**, 319–331 (2014).

[12] Krishnamurthy, L. & Krishnamurthy, V. Indian monsoon's relation with the decadal part of pdo in observations and ncar ccsm4. *International Journal of Climatology* **37**, 1824–1833 (2017). URL https://rmets.onlinelibrary.wiley.com/doi/abs/10.1002/joc.4815. https://rmets.onlinelibrary.wiley.com/doi/pdf/10.1002/joc.4815.

[13] Goswami, B. N., Madhusoodanan, M. S., Neema, C. P. & Sengupta, D. A physical mechanism for north atlantic sst influence on the indian summer monsoon. *Geophysical Research Letters* **33** (2006). URL https://agupubs.onlinelibrary.wiley.com/doi/abs/10.1029/2005GL024803. https://agupubs.onlinelibrary.wiley.com/doi/pdf/10.1029/2005GL024803.

[14] Kumar, K. K., Rajagopalan, B. & Cane, M. A. On the weakening relationship between the indian monsoon and ENSO. *Science* **284**, 2156–2159 (1999).

[15] Saji, N. H., Goswami, B. N., Vinayachandran, P. N. & Yamagata, T. A dipole mode in the tropical indian ocean. *Nature* **401**, 360–363 (1999).

[16] Goswami, B. N. *South Asian monsoon*, 19–61 (Springer Berlin Heidelberg, Berlin, Heidelberg, 2005). URL https://doi.org/10.1007/3-540-27250-X_2.

[17] Taraphdar, S., Zhang, F., Leung, L. R., Chen, X. & Pauluis, O. M. Mjo affects the monsoon onset timing over the indian region. *Geophysical Research Letters* **45**, 10011–10018 (2018). URL https://agupubs.onlinelibrary.wiley.com/doi/abs/10.1029/2018GL078804. https://agupubs.onlinelibrary.wiley.com/doi/pdf/10.1029/2018GL078804.

[18] Borah, P. J., Venugopal, V., Sukhatme, J., Muddebihal, P. & Goswami, B. N. Indian monsoon derailed by a north atlantic wavetrain. *Science* **370**, 1335–1338 (2020).

[19] Pathak, A., Ghosh, S., Martinez, J. A., Dominguez, F. & Kumar, P. Role of oceanic and land moisture sources and transport in the seasonal and interannual variability of summer monsoon in india. *J. Clim.* **30**, 1839–1859 (2017).

[20] McDermid, S. *et al.* Irrigation in the earth system. *Nat. Rev. Earth Environ.* **4**, 435–453 (2023).

[21] Zhou, W. *et al.* Connections between the hydrological cycle and crop yield in the rainfed u.s. corn belt. *Journal of Hydrology* **590**, 125398 (2020). URL https://www.sciencedirect.com/science/article/pii/S0022169420308581.

[22] Alter, R. E., Im, E.-S. & Eltahir, E. A. B. Rainfall consistently enhanced around the gezira scheme in east africa due to irrigation. *Nat. Geosci.* **8**, 763–767 (2015).

[23] Chou, C., Ryu, D., Lo, M.-H., Wey, H.-W. & Malano, H. M. Irrigation-induced land–atmosphere feedbacks and their impacts on indian summer monsoon. *J. Clim.* **31**, 8785–8801 (2018).

[24] Devanand, A., Huang, M., Ashfaq, M., Barik, B. & Ghosh, S. Choice of irrigation water management practice affects indian summer monsoon rainfall and its extremes. *Geophysical Research Letters* **46**, 9126–9135 (2019). URL https://agupubs.onlinelibrary.wiley.com/doi/abs/10.1029/2019GL083875. https://agupubs.onlinelibrary.wiley.com/doi/pdf/10.1029/2019GL083875.

[25] Tuinenburg, O. A., Hutjes, R. W. A., Stacke, T., Wiltshire, A. & Lucas-Picher, P. Effects of irrigation in india on the atmospheric water budget. *Journal of Hydrometeorology* **15**, 1028–1050 (2014). URL http://dx.doi.org/10.1175/JHM-D-13-078.1.

[26] Greve, P. *et al.* Observational evidence of increased afternoon rainfall downwind of irrigated areas. *Nat. Commun.* **16**, 3415 (2025).

[27] Cui, J. *et al.* Global water availability boosted by vegetation-driven changes in atmospheric moisture transport. *Nat. Geosci.* **15**, 982–988 (2022).

[28] Portmann, F. T., Siebert, S. & Döll, P. Mirca2000—global monthly irrigated and rainfed crop areas around the year 2000: A new high-resolution data set for agricultural and hydrological modeling. *Global Biogeochemical Cycles* **24** (2010). URL https://agupubs.onlinelibrary.wiley.com/doi/abs/10.1029/2008GB003435. https://agupubs.onlinelibrary.wiley.com/doi/pdf/10.1029/2008GB003435.

[29] Harding, R., Blyth, E., Tuinenburg, O. & Wiltshire, A. Land atmosphere feedbacks and their role in the water resources of the ganges basin. *Science of The Total Environment* **468–469**, S85–S92 (2013). URL http://dx.doi.org/10.1016/j.scitotenv.2013.03.016.

[30] Tuinenburg, O. A., Hutjes, R. W. A. & Kabat, P. The fate of evaporated water from the ganges basin. *Journal of Geophysical Research: Atmospheres* **117** (2012). URL http://dx.doi.org/10.1029/2011JD016221.

[31] Allen, R. G., Pereira, L. S., Raes, D. & Smith, M. *Crop evapotranspiration: Guidelines for computing crop water requirements.* No. 56 in FAO Irrigation and drainage paper (Food and Agriculture Organization of the United Nations, Rome, Italy, 1998).

[32] Bonetti, S., Sutanudjaja, E. H., Mabhaudhi, T., Slotow, R. & Dalin, C. Climate change impacts on water sustainability of south african crop production. *Environ. Res. Lett.* **17**, 084017 (2022).

[33] Stohl, A., Forster, C., Frank, A., Seibert, P. & Wotawa, G. Technical note: The lagrangian particle dispersion model flexpart version 6.2. *Atmospheric Chemistry and Physics* **5**, 2461–2474 (2005). URL https://acp.copernicus.org/articles/5/2461/2005/.

[34] Pisso, I. *et al.* The lagrangian particle dispersion model FLEXPART version 10.4. *Geosci. Model Dev.* **12**, 4955–4997 (2019).

[35] Hersbach, H. *et al.* The era5 global reanalysis. *Quarterly Journal of the Royal Meteorological Society* **146**, 1999–2049 (2020). URL https://rmets.onlinelibrary.wiley.com/doi/abs/10.1002/qj.3803. https://rmets.onlinelibrary.wiley.com/doi/pdf/10.1002/qj.3803.

[36] Keune, J., Schumacher, D. L. & Miralles, D. G. A unified framework to estimate the origins of atmospheric moisture and heat using lagrangian models. *Geoscientific Model Development* **15**, 1875–1898 (2022). URL https://gmd.copernicus.org/articles/15/1875/2022/.

[37] Beck, H. E. *et al.* MSWEP V2 global 3-hourly 0.1° precipitation: Methodology and quantitative assessment. *Bull. Am. Meteorol. Soc.* **100**, 473–500 (2019).

[38] Miralles, D. G. *et al.* GLEAM4: global land evaporation and soil moisture dataset at 0.1 resolution from 1980 to near present. *Sci. Data* **12**, 416 (2025).

[39] Yu, L. & Weller, R. A. Objectively analyzed air–sea heat fluxes for the global ice-free oceans (1981–2005). *Bulletin of the American Meteorological Society* **88**, 527 – 540 (2007). URL https://journals.ametsoc.org/view/journals/bams/88/4/bams-88-4-527.xml.

[40] Tuninetti, M., Tamea, S. & Dalin, C. Water debt indicator reveals where agricultural water use exceeds sustainable levels. *Water Resources Research* **55**, 2464–2477 (2019). URL https://agupubs.onlinelibrary.wiley.com/doi/abs/10.1029/2018WR023146. https://agupubs.onlinelibrary.wiley.com/doi/pdf/10.1029/2018WR023146.

[41] Navale, A. & Karthikeyan, L. Understanding recycled precipitation at different spatio-temporal scales over india: An eulerian water tagging approach. *Water Resources Research* **59**, e2022WR032605 (2023). URL https://agupubs.onlinelibrary.wiley.com/doi/abs/10.1029/2022WR032605. E2022WR032605 2022WR032605, https://agupubs.onlinelibrary.wiley.com/doi/pdf/10.1029/2022WR032605.

[42] Pathak, A., Ghosh, S. & Kumar, P. Precipitation recycling in the indian subcontinent during summer monsoon. *J. Hydrometeorol.* **15**, 2050–2066 (2014).

[43] Kar, G. & Kumar, A. Evaluation of post-rainy season crops with residual soil moisture and different tillage methods in rice fallow of eastern india. *Agricultural Water Management* **96**, 931–938 (2009). URL https://www.sciencedirect.com/science/article/pii/S0378377409000031.

[44] Kholová, J., McLean, G., Vadez, V., Craufurd, P. & Hammer, G. L. Drought stress characterization of post-rainy season (rabi) sorghum in india. *Field Crops Research* **141**, 38–46 (2013). URL https://www.sciencedirect.com/science/article/pii/S0378429012003681.

[45] Pantha, S., Kilian, B., Özkan, H., Zeibig, F. & Frei, M. Physiological and biochemical changes induced by drought stress during the stem elongation and anthesis stages in the triticum genus. *Environmental and Experimental Botany* **228**, 106047 (2024). URL https://www.sciencedirect.com/science/article/pii/S0098847224004052.

[46] Abid, M. *et al.* Nitrogen nutrition improves the potential of wheat (triticum aestivum l.) to alleviate the effects of drought stress during vegetative growth periods. *Frontiers in Plant Science* **Volume 7 - 2016** (2016). URL https://www.frontiersin.org/journals/plant-science/articles/10.3389/fpls.2016.00981.

[47] Yang, J. & Zhang, J. Grain filling of cereals under soil drying. *New Phytologist* **169**, 223–236 (2006). URL https://nph.onlinelibrary.wiley.com/doi/abs/10.1111/j.1469-8137.2005.01597.x. https://nph.onlinelibrary.wiley.com/doi/pdf/10.1111/j.1469-8137.2005.01597.x.

[48] BARNABÁS, B., JÄGER, K. & FEHÉR, A. The effect of drought and heat stress on reproductive processes in cereals. *Plant, Cell & Environment* **31**, 11–38 (2008). URL https://onlinelibrary.wiley.com/doi/abs/10.1111/j.1365-3040.2007.01727.x. https://onlinelibrary.wiley.com/doi/pdf/10.1111/j.1365-3040.2007.01727.x.

[49] Chatterjee, S., Lamba, R. & Zaveri, E. D. The role of farm subsidies in changing india's water footprint. *Nat. Commun.* **15**, 8654 (2024).

[50] Singh, G., Gandhi, V. P. & Jain, D. Micro-irrigation adoption and the jevons' paradox: A study from four states of india. *Agricultural Water Management* **303**, 109040 (2024). URL https://www.sciencedirect.com/science/article/pii/S0378377424003755.

[51] Rockström, J. *et al.* Managing water in rainfed agriculture—the need for a paradigm shift. *Agricultural Water Management* **97**, 543–550 (2010). URL https://www.sciencedirect.com/science/article/pii/S0378377409002789. Comprehensive Assessment of Water Management in Agriculture.

[52] Mehta, P. *et al.* Half of twenty-first century global irrigation expansion has been in water-stressed regions. *Nature Water* **2**, 254–261 (2024). URL http://dx.doi.org/10.1038/s44221-024-00206-9.

[53] McDermid, S. S., Mearns, L. O. & Ruane, A. C. Representing agriculture in earth system models: Approaches and priorities for development. *Journal of Advances in Modeling Earth Systems* **9**, 2230–2265 (2017). URL http://dx.doi.org/10.1002/2016MS000749.

[54] Yao, Y. *et al.* Implementation and evaluation of irrigation techniques in the community land model. *Journal of Advances in Modeling Earth Systems* **14** (2022). URL http://dx.doi.org/10.1029/2022MS003074.

[55] Devanand, A., Huang, M., Ashfaq, M., Barik, B. & Ghosh, S. Choice of irrigation water management practice affects indian summer monsoon rainfall and its extremes. *Geophysical Research Letters* **46**, 9126–9135 (2019). URL http://dx.doi.org/10.1029/2019GL083875.

[56] Schmitt, R. J. P., Rosa, L. & Daily, G. C. Global expansion of sustainable irrigation limited by water storage. *Proceedings of the National Academy of Sciences* **119** (2022). URL http://dx.doi.org/10.1073/pnas.2214291119.

[57] Koppa, A. Data: Widespread reliance of rainfed crops on upwind irrigated agriculture in india (2025). URL https://doi.org/10.5281/zenodo.17238979.

[58] Sodemann, H., Masson-Delmotte, V., Schwierz, C., Vinther, B. M. & Wernli, H. Interannual variability of greenland winter precipitation sources: 2. effects of north atlantic oscillation variability on stable isotopes in precipitation. *Journal of Geophysical Research: Atmospheres* **113** (2008). URL https://agupubs.onlinelibrary.wiley.com/doi/abs/10.1029/2007JD009416. https://agupubs.onlinelibrary.wiley.com/doi/pdf/10.1029/2007JD009416.

[59] Emanuel, K. A. A scheme for representing cumulus convection in large-scale models. *Journal of Atmospheric Sciences* **48**, 2313 – 2329 (1991). URL https://journals.ametsoc.org/view/journals/atsc/48/21/1520-0469_1991_048_2313_asfrcc_2_0_co_2.xml.

[60] Sodemann, H. Beyond turnover time: Constraining the lifetime distribution of water vapor from simple and complex approaches. *Journal of the Atmospheric Sciences* **77**, 413 – 433 (2020). URL https://journals.ametsoc.org/view/journals/atsc/77/2/jas-d-18-0336.1.xml.

Supplementary Material

Widespread reliance of rainfed crops on upwind irrigated agriculture in India

Akash Koppa[1,2*], Francesca Bassani[1], Jessica Keune[3], Victoria Deman[4], Damian Insua-Costa[4], Vittal Hari[5], Subimal Ghosh[6], Diego G. Miralles[4], and Sara Bonetti[1,*]

[1]Laboratory of Catchment Hydrology and Geomorphology, School of Architecture, Civil and Environmental Engineering, EPFL Valais Wallis, Sion, Switzerland

[2]Department of Environmental Science & Technology, University of Maryland, College Park, United States

[3]European Centre for Medium-Range Weather Forecasts, Bonn, Germany

[4]Hydro-Climate Extremes Lab (H-CEL), Ghent University, Ghent, Belgium

[5]Department of Environmental Science and Engineering, Indian Institute of Technology (ISM) Dhanbad, Dhanbad, India

[6]Department of Civil Engineering, Indian Institute of Technology Bombay, Mumbai, India

[*]Corresponding author, emails: sara.bonetti@epfl.ch and akoppa@umd.edu

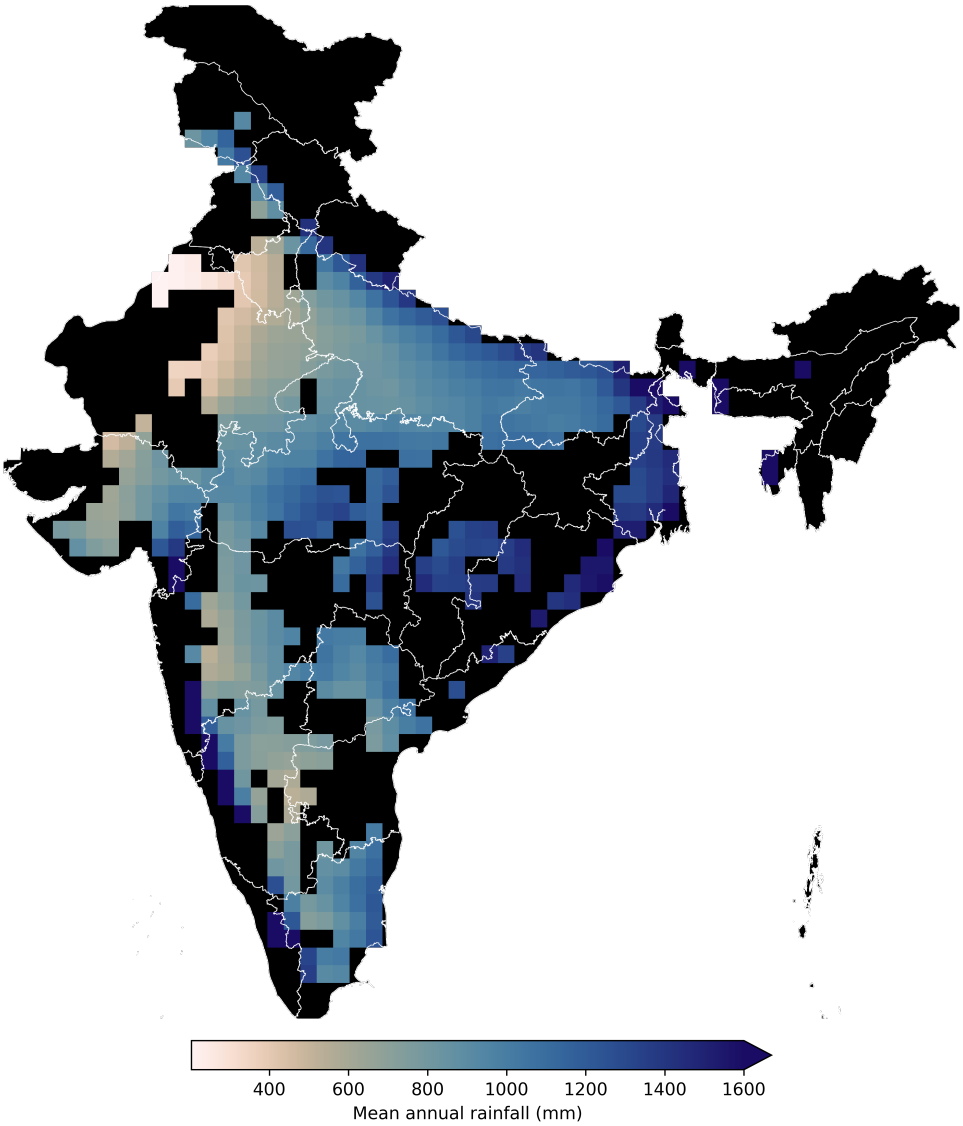

Figure S1: Map of India showing the mean annual rainfall over rainfed regions, estimated over the years 2000–2020.

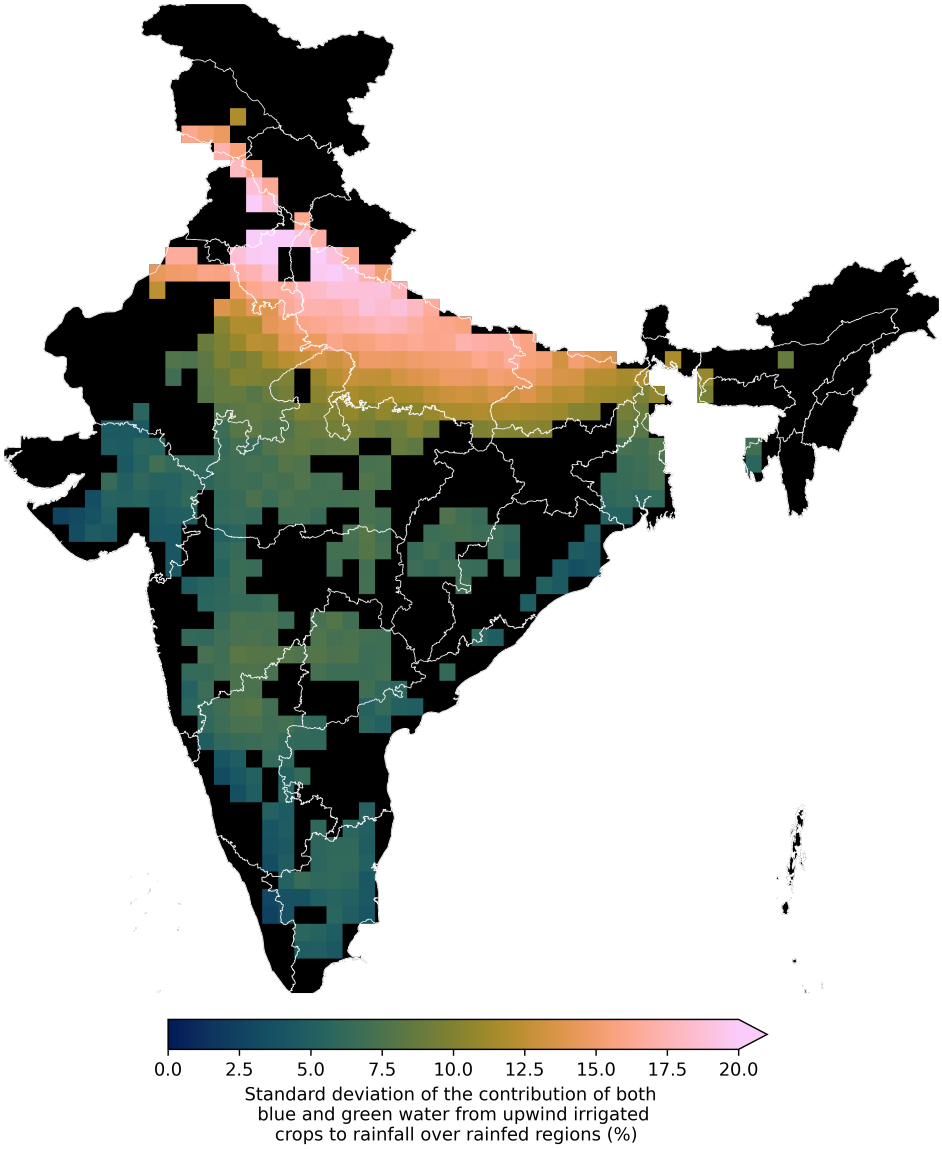

Figure S2: Map of India showing the standard deviation of the contribution of evaporation from upwind irrigated crops (both green and blue water) to rainfall over rainfed regions, estimated over the years 2000–2020.

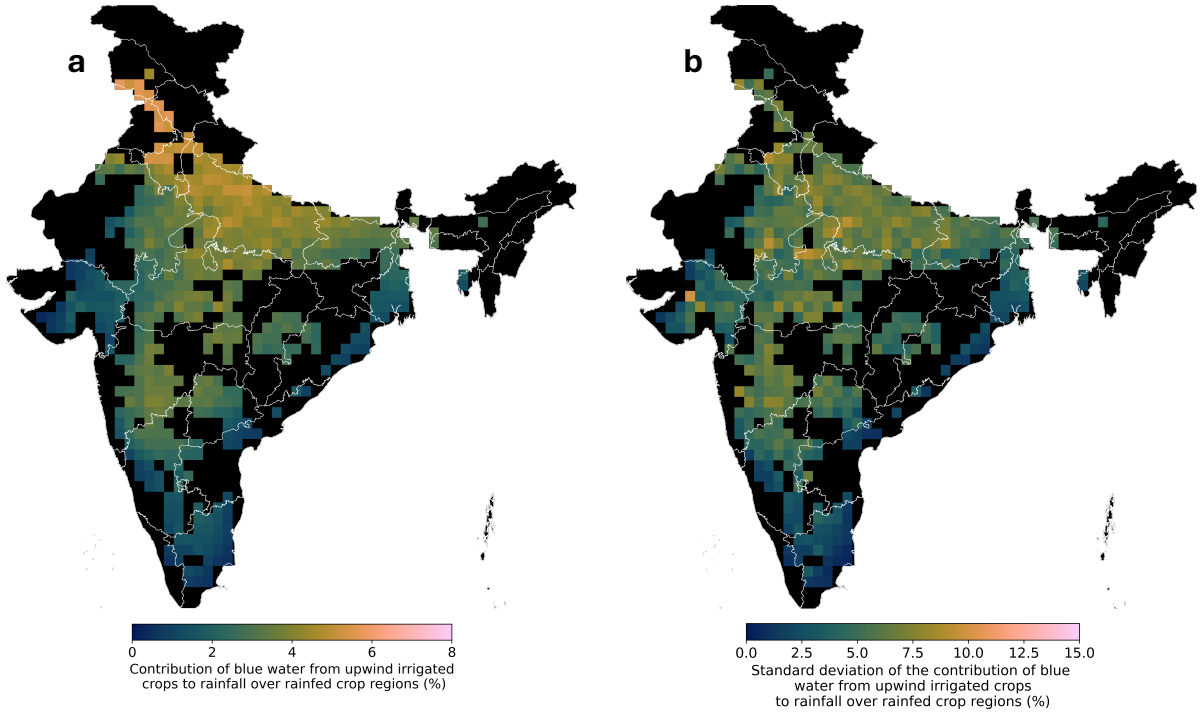

Figure S3: Map of India showing the (a) actual and (b) standard deviation of the contribution of evaporation from upwind irrigation (only blue water) to rainfall over rainfed regions, estimated over the years 2000–2020.

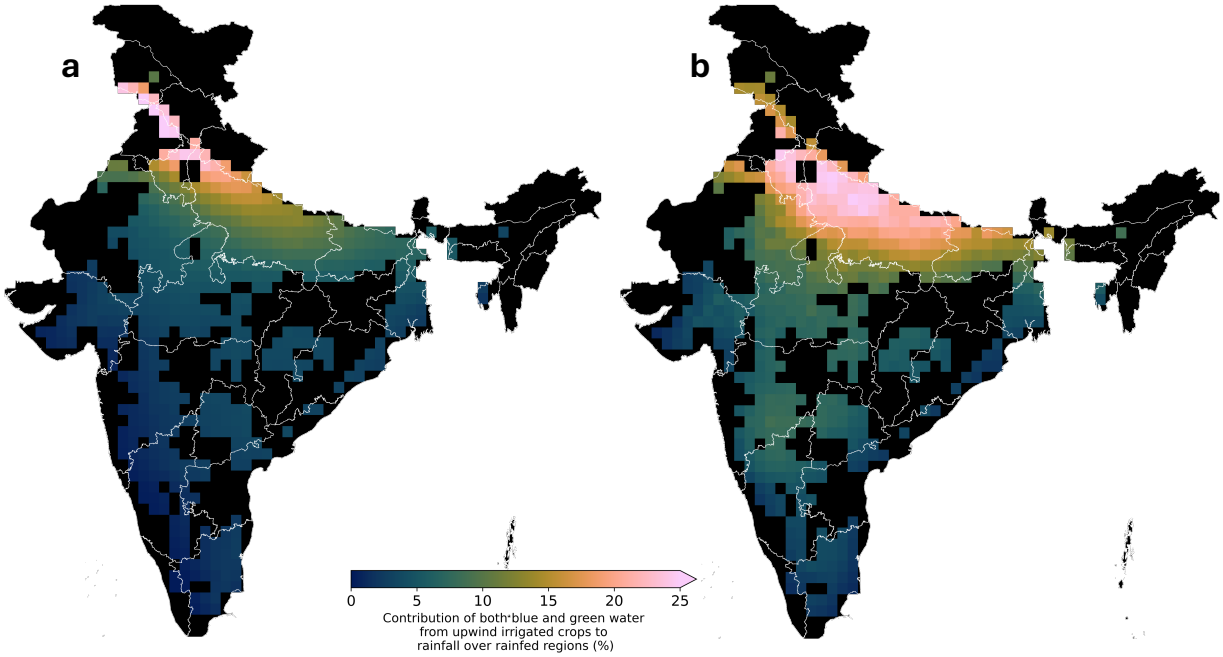

Figure S4: Map of India showing the contribution of evaporation from upwind irrigated crops (both green and blue water) to rainfall over rainfed regions, during (a) the monsoon (June–September) and (b) the non-monsoon seasons, estimated over the years 2000–2020.

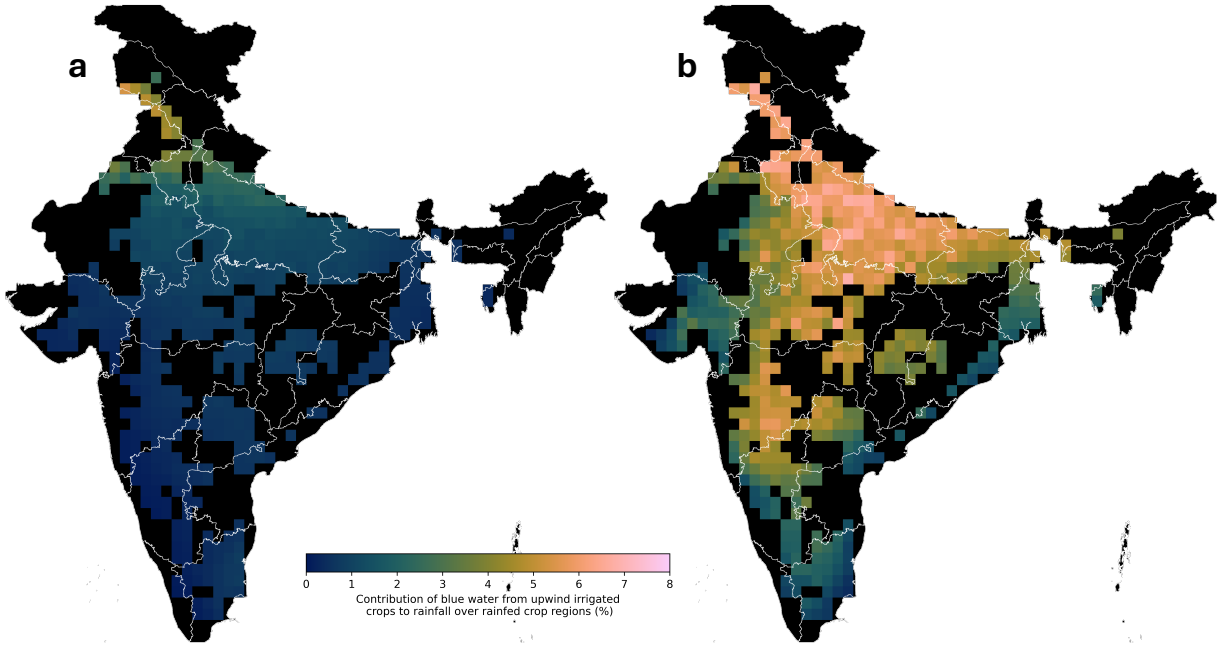

Figure S5: Map of India showing the contribution of evaporation from upwind irrigation (only blue water) to rainfall over rainfed regions, during (a) the monsoon (June–September) and (b) the non-monsoon seasons, estimated over the years 2000–2020.

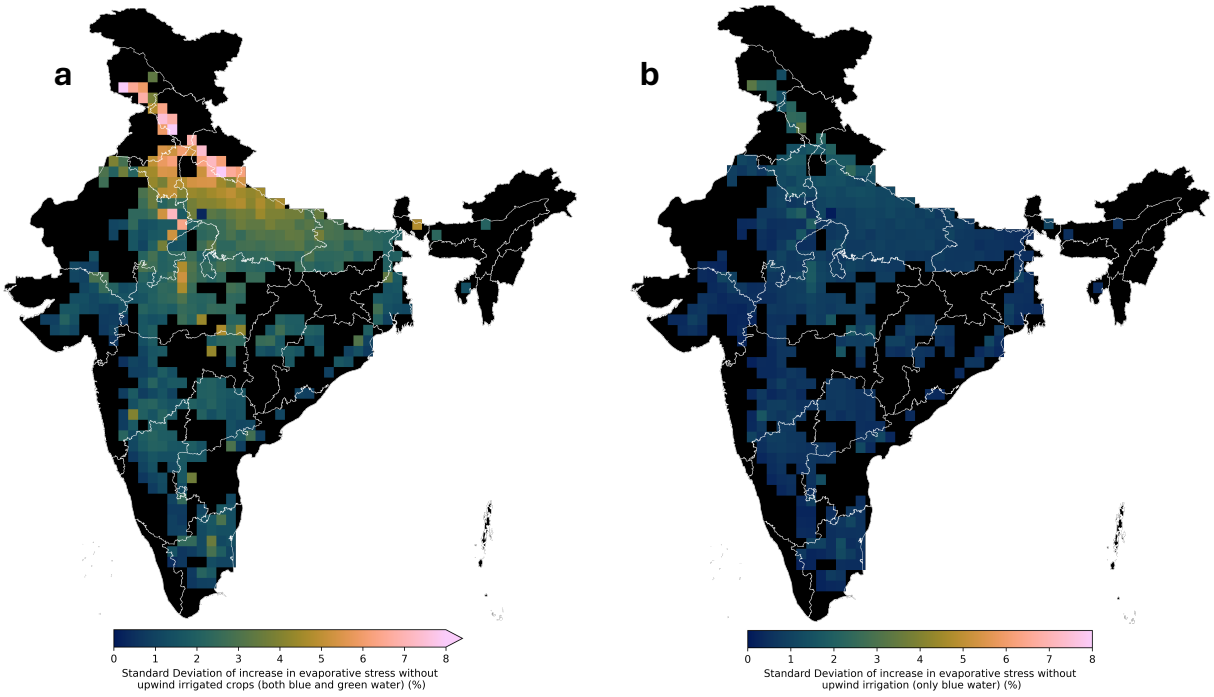

Figure S6: Map of India showing the standard deviation of the increase in evaporative stress in rainfed crops due to the absence of upwind (a) irrigated crops (blue and green water) and (b) irrigation (blue water), estimated over the years 2000–2020.

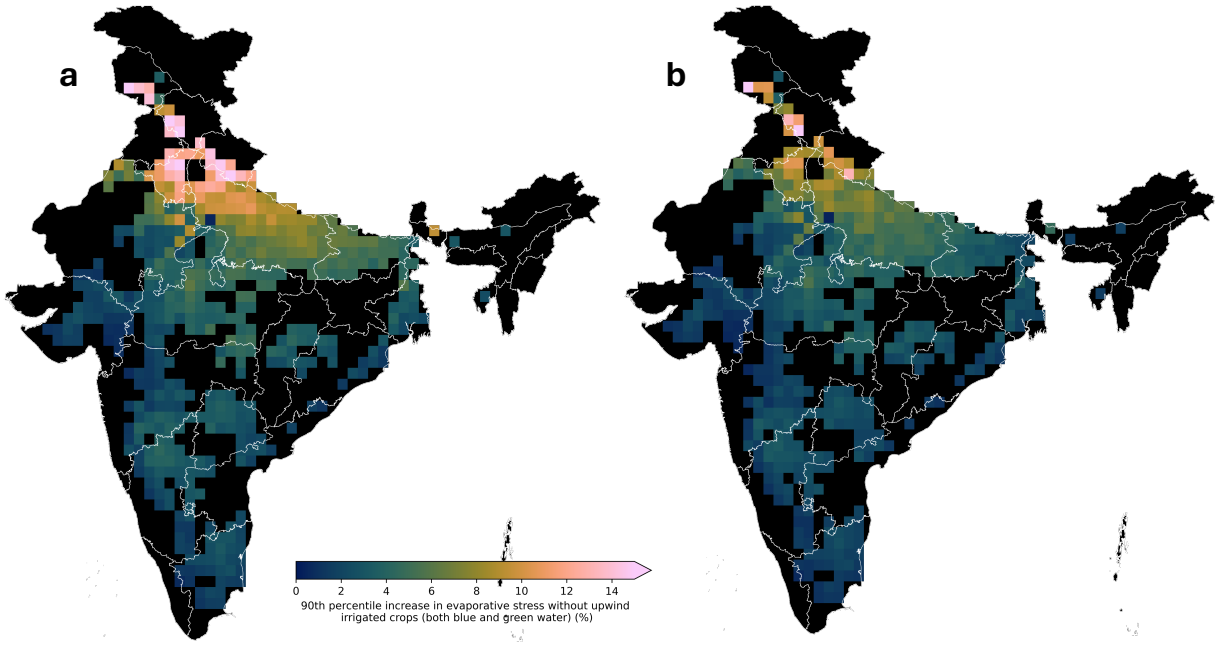

Figure S7: Map of India showing the 90th percentile increase in evaporative stress in rainfed crops due to the absence of upwind (a) irrigated crops (blue and green water) and (b) irrigation (blue water), estimated over the years 2000–2020.